Dalton Transactions

ROYAL SOCIETY OF CHEMISTRY

PAPER

View Article Online
View Journal | View Issue

Cite this: *Dalton Trans.*, 2024, **53**, 18880

Quantitative determination and subcellular mapping of Pt-based drugs in single breast tumour cells *via* laser ablation-ICP-mass spectrometry†

Legna Colina-Vegas, [a] Thibaut Van Acker, [b] Wilmer Villarreal,[a] Olivier De Wever,[c] Alzir Azevedo Batista, [d] Joaquim Araújo Nóbrega [d] and Frank Vanhaecke *[b]

Received 30th August 2024,
Accepted 18th October 2024

DOI: 10.1039/d4dt02467b

rsc.li/dalton

For years, cancer has been the second cause of death worldwide, preceded by cardiovascular diseases only. The number of research groups focusing on the discovery of new drugs to treat cancer is growing and the aim is to look for more effective compounds that cause less severe side effects and do not suffer from therapeutic resistance. The metal complexes cisplatin and carboplatin are widely used in the chemotherapeutic treatment of various types of cancer, including triple-negative breast cancer (TNBC). Both compounds are essential in modern chemotherapy and continue to be the subject of research to optimize their therapeutic properties and minimize adverse effects. Laser ablation-inductively coupled plasma-mass spectrometry (LA-ICP-MS) allows obtaining both quantitative data and information on the spatial distribution of elements in biological tissues and populations of single cells. In this work, the content of Pt and its distribution in TNBC MDA-MB-231 cells were determined *via* LA-ICP-MS analysis after incubation with different Pt-containing drugs. The quantitative analysis of single cells and the elemental maps revealing the distribution of Pt over and within the cells provide an enhanced insight into the potential mechanism of action of these Pt-containing drugs and their efficacy against TNBC.

Introduction

In accordance with the National Institutes of Health (NIH), cancer is the name given to a collection of related diseases. In all types of cancer, some of the body's cells begin to divide without stopping and spread into surrounding tissues.[1]

Normally, human cells grow and divide to form new cells as the body needs them. When cells grow old or become damaged, they die, and new cells take their place. When cancer develops, however, this orderly process breaks down. As cells become more and more abnormal, old or damaged, they survive when they should die, and new cells form when they are not needed. These extra cells can divide without stopping and may form tumours and invade other tissues. The process by which a normal cell acquires tumour characteristics occurs through mutations and epigenetic changes that activate oncogenesis or inhibit the activity of tumour suppressor genes. Auto-sufficiency in signals of growth, resistance to inhibitory signals of growth and resistance to cell death allowing replicative immortality and induction of angiogenesis are among the physiological alterations that a tumour cell presents. In 2022, about 9.7 million people died from cancer and there were about 20 million new diagnoses.[2]

Since decades, chemotherapeutic agents and ionizing radiation are the treatments most often used to eliminate primary cancer. These therapies provide significant benefit and can cure some cases of cancer, but the incidence of tumour recurrence is a problem arising from the development of resistance by tumour cells to chemotherapeutic agents. Therefore, the quest for new compounds capable of treating and eliminating the resistant tumour cells must be continued.[3]

Metal complexes offer many advantages compared to conventional organic compounds in the development of potential medicinal compounds. These advantages are due to their ability to coordinate with ligands in a three-dimensional configuration, thus allowing functionalization of groups that can be tailored to defined molecular targets. Pt-containing drugs, such as cisplatin and carboplatin, remain among the most widely utilized types of drugs in chemotherapy treatment used for various cancers such as ovarian, bladder, lung, and testicular cancer, among others. The widely accepted mechanism of

[a]*Federal University of Rio Grande do Sul, Institute of Chemistry, Brazil*
[b]*Ghent University, Department of Chemistry, Atomic & Mass Spectrometry – A&MS Research Group, Belgium. E-mail: frank.vanhaecke@ugent.be*
[c]*Ghent University, Department of Human Structure and Repair, Laboratory of Experimental Cancer Research, Belgium*
[d]*Federal University of São Carlos, Department of Chemistry, Brazil*
†Electronic supplementary information (ESI) available. See DOI: https://doi.org/10.1039/d4dt02467b

action of these platinum drugs includes their internalization into cells primarily through passive diffusion and the transporter protein CTR1. In the intracellular medium, the neutral cisplatin structure changes to a positively charged platinum complex as a consequence of hydrolysis. These complexes are highly reactive and interact with cellular DNA, leading to the formation of Pt-DNA covalent binding. The crosslinks thus formed disrupt the DNA structure and function, ultimately triggering apoptosis or a novel cell death mechanism known for cisplatin: ferroptosis.[4]

For non-luminescent complexes, a variety of techniques have been developed and used to visualize the occurrence of metal ions in biological samples in a way that preserves their spatial distribution.

This can be done for either fixed or live specimens. A suite of analytical techniques capable of revealing the metal distribution, including secondary ion mass spectrometry (SIMS), laser ablation-inductively coupled plasma-mass spectrometry (LA-ICP-MS), electron spectroscopy imaging (ESI) combined with electron energy loss spectroscopy (EELS), and X-ray fluorescence microscopy (XRFM), have been applied to fixed biological specimens. Each of these techniques allows researchers to determine the total metal content with high sensitivity and reveal the sub-cellular spatial distribution. Some research groups have taken advantage of this to study luminescent and non-luminescent metal complexes.[5]

LA-ICP-MS is a well-established technique that enables sensitive elemental and/or isotopic analysis, as well as elemental mapping performed directly on solid samples. LA-ICP-MS is characterized by low detection limits, high spatial resolution, full elemental mass spectrum coverage, limited sample preparation, and a wide linear dynamic range. For analysis, a high-energy UV laser beam is focused on the sample surface and upon interaction of the laser pulse with the sample material, a small amount is vaporized creating an aerosol with fine particles upon condensation – a process known as laser ablation. The laser-generated sample particles are then transported into the ICP ion source of the ICP-mass spectrometer for atomization and subsequent ionization of the atoms thus formed. The ions generated in the plasma torch are extracted using an interface and introduced into a mass spectrometer for both elemental and isotopic analysis.[6]

Elemental mapping using LA-ICP-MS (often referred to as imaging) has advanced the bio-analytical field.[7] Imaging of single cells using this technique can provide significant information concerning the uptake and distribution of metals, identification of metabolic routes, and the translocation of metals and their release. Such information is significant in pharmaceutical research aiming at the improvement of existing drugs and the development of new ones. The technique has, *e.g.*, been used successfully to determine the distribution of Ag and Au nanoparticles[8] within individual fibroblast cells and for the quantitative determination of Al in lung epithelial cells and skin keratinocytes grown on glass slides.[9] The uptake of a ^{165}Ho-tagged compound was evaluated using LA-ICP-MS imaging in MDA-MB-231 cells and MDA-MB-231 X4 cells.[10] The ^{165}Ho-containing compound showed a clear uptake in MDA-MB-231 X4 cells, indicating specificity for the CXCR4 receptor.[11] Recent studies using LA-ICP-MS include the study of the oxaliplatin distribution in lung tumour cells.[12] In the present study, we have investigated the uptake and intracellular distribution of Pt in TNBC MDA-MB-231 cells after incubation with either cisplatin, carboplatin or a new Pt-phosphine complex.

Results and discussion

Synthesis and characterization

A new platinum(II) clotrimazole complex was synthesized by reaction of the clotrimazole (CTZ) molecule with precursors, having the general formula *cis*-[Pt(PPh$_3$)$_2$Cl$_2$], as displayed in Scheme 1. The result of elemental analysis of this complex agreed with the proposed molecular formula with a bias of less than 0.4%. The molar conductivity values obtained for the complex are in the range for a 1 : 1 ratio of electrolyte dissolved in acetone.[8] In the IR spectra, the characteristic bands of CTZ and phosphine ligands are observed, such as ν(C–H aromatic) 3085 cm^{-1}, ν(C=N) 1572 cm^{-1} and ν(C=C) 1510 cm^{-1}, together with the bands corresponding to counter-ions, ν(P–F) 840 cm^{-1} and δ(P–F) 557 cm^{-1}. The far-infrared (FIR) spectra of the complex display a band at ν(Pt–P) 518 cm^{-1}, probably overlapping with ν(Pt–N) and ν(Pt–Cl) 312 cm^{-1}.

All NMR signals could be assigned based on one-dimensional (1D) and two-dimensional (2D) correlation spectroscopy (COSY). The ^{1}H NMR spectrum displayed all the signals corresponding to phosphine and CTZ ligands, and the relative inte-

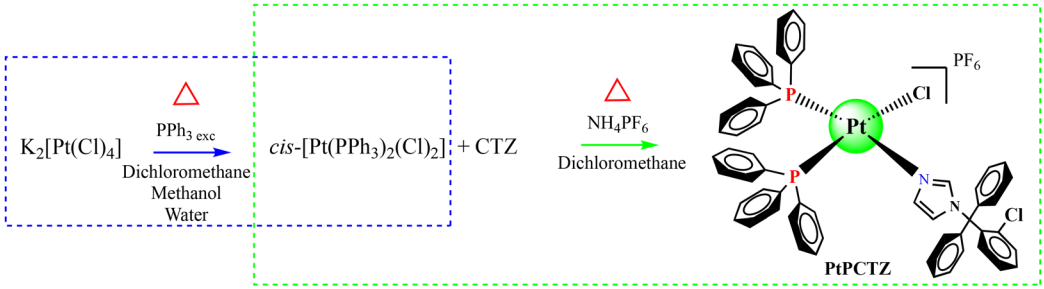

Scheme 1 Synthetic route for the platinum-clotrimazole complex and its precursor using Schlenk techniques.

grals corresponded to two phosphine ligands for one CTZ molecule. In the $^{31}P\{^{1}H\}$ NMR spectrum of the PtPCTZ complex, two doublets were observed, indicating the presence of two magnetically different P atoms coordinated to the Pt metal center. One of the P atoms at 4.73 ppm was in the *trans* position with respect to the Cl atom (P_a), and the other (P_b) was more shielded in the *trans* position with respect to the N atom of the CTZ. All signals were flanked by satellite peaks of the respective multiplicity with an intensity of ~1 : 4 : 1 generated because of the coupling of the P atoms with the ^{195}Pt nuclide.

Effect of platinum-based drugs on the morphology and viability of TNBC MDA-MB-231 cells

Prior to quantification and subcellular mapping by LA-ICP-MS, MDA-MB-231 cells were incubated with different concentrations of PtPCTZ, cisplatin or carboplatin for 24 h, after which the cell viability was determined using an MTT assay. These tests aimed at identifying the best conditions for further testing. For successful cell culture experiments, routine analysis of the cell morphology (*i.e.*, evaluating their shape and appearance) is an essential step. In the treatment with toxic substances like metal drugs, signs of cell deterioration can include the occurrence of round cells, damage to the cell body, granularity around the nucleus, detachment of the cells from the substrate, cytoplasmic vacuolation and a decrease in confluence. All these changes in the basic cellular morphology should show a clear concentration-dependent response. Allowing the effects to progress too far, will make them irreversible and cause cell death, defaulting the detection by LA-ICP-MS.

The effect of the treatment with the platinum-based drugs on the morphology can be observed in Fig. 1. The MDA-MB-231 cell line grew as a monolayer when cultured under normal conditions, presenting the morphology of epithelial-like cells. The cell layer is attached to the substrate and is wider in the middle and tapered at both ends. This is called "spindle-shaped" and is the common morphology for this cell line. After 24 h of incubation, the cells treated with PtPCTZ, cisplatin or carboplatin, especially at higher concentrations, have been found to be mostly spherically shaped, demonstrating damaged cell bodies and a loss of adhesion and confluence. This result suggests a clear change in the cell morphology induced by the cytotoxic complexes, indicating cell death by an apoptosis pathway, as confirmed by flow cytometry measurements of cisplatin and carboplatin in the treated MDA-MB-231 cells.[12,13]

Based on the morphological observations, the concentrations selected for cell preparation were: 7.0 μmol L^{-1} of PtPCTZ and 30 μmol L^{-1} of cisplatin or carboplatin. The cellular viability after treatment was evaluated using the MTT assay relying on UV-Vis spectrometry. ESI Fig. S1† provides the cell viability percentage after exposure to the platinum complexes. The values range between 75 and 87%, confirming that the selected concentrations do not substantially affect cell growth and can be used in the context of subsequential analysis of tumour cells *via* LA-ICP-MS.

Determination of Pt in individual cells using single-cell LA-ICP-MS

Cell samples prepared for LA-ICP-MS should have a flat area and good adherent properties with respect to the support material. Thus, cell sample preparation for LA-ICP-MS consisted of a fixation process followed by dehydration of the sample. The fixation step allows keeping the cellular components as "life-like" as possible because all biochemical and proteolytic processes are inactivated, and the structure is immobilized and locked. Fixation of biological samples can be achieved by chemical or physical means. Physical methods are more common for tissues and include heating, microwaving and cryopreservation. Chemical fixation is usually achieved by immersing the specimen in a fixative solution containing a single fixative agent dissolved in water, alcohol or a buffer solution to stabilize the pH. Polyoxymethylene, commonly known as paraformaldehyde (PFA), was used in this work. It is a frequently used crosslinking fixative in histology and is formed by the condensation of the predominant species

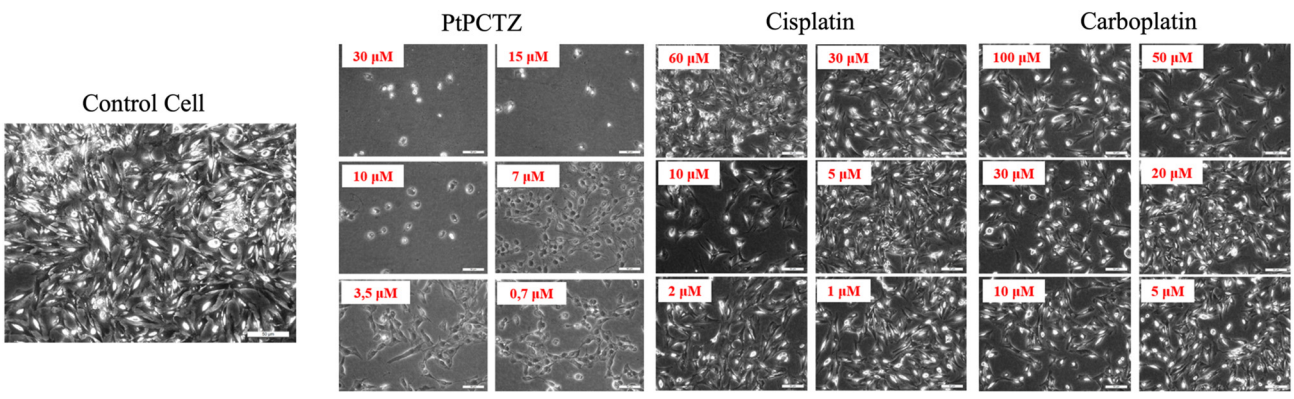

Fig. 1 Cellular morphology of MDA-MB-231 without treatment (control cells) and after treatment with different platinum-based drugs at several concentrations for 24 h to select the best cell preparation conditions for LA-ICP-MS. Scale bar 50 μm.

methanediol in solutions of formaldehyde at equilibrium (Scheme S1†).

The chemical fixative can react with nitrogen and some other atoms of proteins forming a cross-linking $-CH_2-$ called a methylene bridge.[14]

After fixation, the cells were dehydrated by using a graded series of ethanol to replace water and to remove diffusible ions such as K^+, Na^+, Mg^{2+}, Ca^{2+} and Cl^-. Images of the same cells before and after fixation and dehydration were recorded using an inverted microscope (Fig. 2). The images show that after the fixation and dehydration process, the cells maintain their morphological appearance and no rupturing of the cell membrane was observed, even not 15 days after the procedure.

The platinum uptake by single MDA-MB-231 cells upon incubation with PtPCTZ, cisplatin or carboplatin drugs was quantified by LA-ICP-MS using external calibration based on homogeneous gelatin droplet standards with a concentration range of 0.1–100 ng mg^{-1} Pt. The correlation coefficient of the calibration curve was found to show a good linear fit with r^2 = 1.000 for ^{195}Pt. The ablation crater volumes were determined by interferometric measurements and allowed to express the calibration curve in absolute masses of Pt, as shown in Fig. 3.

The cells shown in Fig. 4 were quantitatively ablated by firing a burst of consecutive laser shots at a laser repetition rate of 250 Hz, thereby generating one transient signal per ablated cell. A laser beam with a circular diameter of 20 μm was used and the laser energy density was set at 0.22 J cm^{-2}. These conditions guaranteed total ablation of each individual cell without co-ablation of the substrate. In this manner, each transient signal observed is representative for the total amount of platinum in the individual cell targeted.[15]

Upon ablation of the control cells, not incubated with platinum-based drugs, the $^{195}Pt^+$ transient signal did not differ from the corresponding blank, as expected for exogenous metals like Pt. While for analysis of 100 individual MDA-MB-231 cells after incubation with one of the Pt complexes, 100 peaks were detected and the $^{195}Pt^+$ signals were integrated for each event, resulting in the data shown in Fig. 5 and Table 1, confirming significant uptake of Pt by TNBC MDA-MB-231 cells. The differences in the Pt uptake from one cell to the other are due to several factors, such as variability

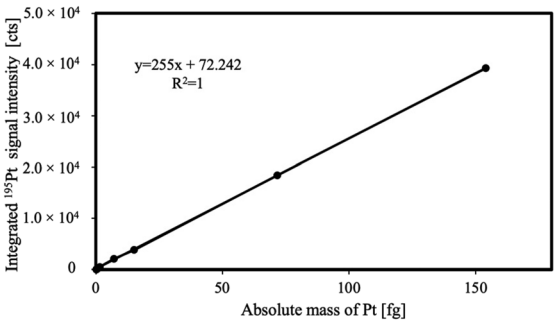

Fig. 3 Calibration curve obtained for ^{195}Pt by LA-ICP-MS analysis of homogeneous gelatin standards.

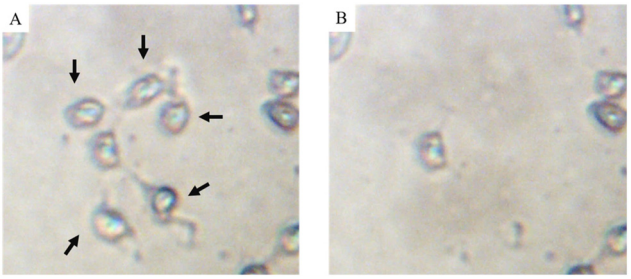

Fig. 4 MDA-MB-231 cells mounted on a glass substrate (A) before and (B) after ablation of single cells.

in size and morphology, as previously demonstrated in Fig. 2, and differences in cellular metabolism.[16]

Additionally, a very important factor could be the cell cycle phase. During the G1 phase, cells prepare for DNA synthesis, and the amount of DNA is relatively low. In the S phase, DNA replication occurs, leading to an increase in DNA content. The G2 phase follows, in which the cell doubles the amount of DNA compared to that in the G1 phase as it prepares for mitosis. Finally, during the M phase, the cell undergoes division, resulting in two daughter cells with identical DNA content.[17]

This variability in Pt content due to cell cycle differences further underscores the complexity of platinum uptake and its

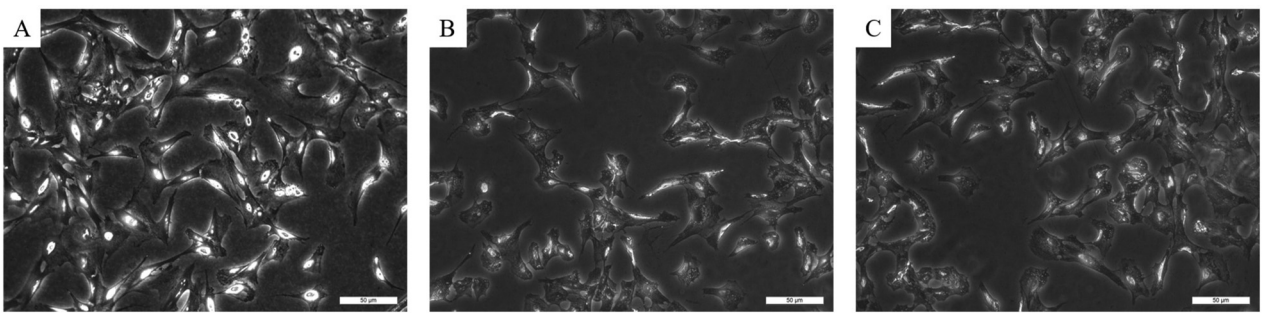

Fig. 2 Effects of fixation and dehydration on cell morphology. (A) Before the procedure, (B) after the procedure and (C) 15 days after the procedure. The scale bar is 50 μm.

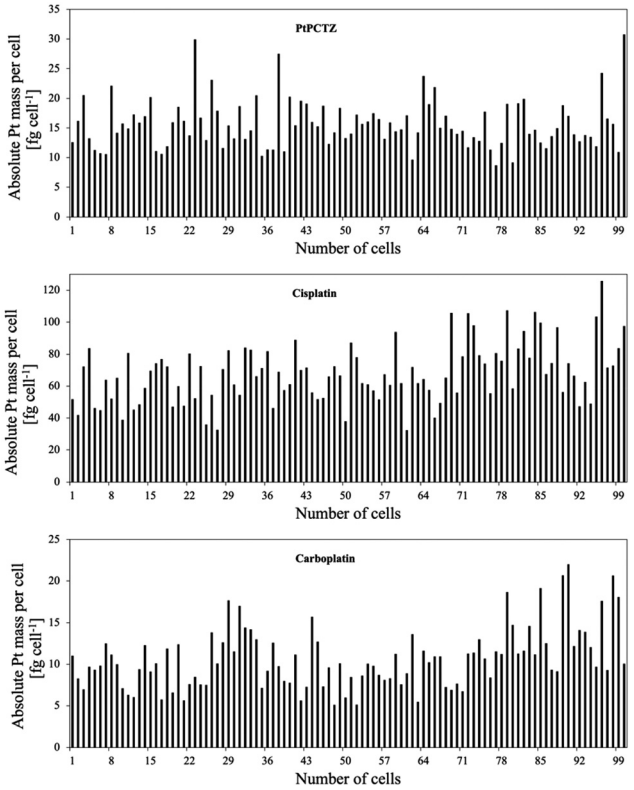

Fig. 5 Absolute masses of Pt per cell as determined by SC-LA-ICP-MS in a population of 100 MDA-MB-231 cells after 24 h of incubation with 7 μmol L^{-1} of PtPCTZ or 30 μmol L^{-1} of cisplatin or carboplatin.

Table 1 Average cellular amounts of Pt in individual MDA-MB-21 cells after exposure to metal-based drugs, expressed in fg per cell determined in n = 3 independent experiments with 100 cells

Cell culture conditions		
Cells exposed to	Concentration [μmol L^{-1} Pt]	LA-ICP-MS analysis fg Pt per cell[1]
PtPCTZ	7.0	16.2 ± 4.6
Cisplatin	30.0	74.0 ± 19.6
Carboplatin	30.0	13.3 ± 4.2

intracellular interactions. Table 1 shows Pt content data (average ± standard deviation) of 100 tumour cells expressed in fg per cell (obtained by also relying on the interferometric data).

The platinum MDA-MB-231 uptake after 24 h of incubation with PtPCTZ, cisplatin and carboplatin was on average 16.2 ± 4.6, 74.0 ± 19.6 and 13.2 ± 4.2 fg Pt per cell, respectively. Our results agree with previous publications reporting on the Pt uptake in tumour cell lines after incubation with cisplatin at concentrations between 3 and 50 μM, as determined using ICP-OES, ICP-MS or SC-ICP-MS techniques. Published results revealed an average Pt concentration of 0.9 fg Pt per SW180 cell,[18] 3.5 fg Pt per A2780 cell,[19] 30 fg Pt per HCT-116 cell[20] and 148 fg Pt per MCF-7 cell.[21]

Revealing the spatial distribution of Pt in cells using LA-ICP-MS

The cellular uptake of the drug alone is insufficient to show biological activity; any potential metallodrug or therapeutic agent must also be able to reach its target within the cell. Mass spectrometry-based cell imaging techniques allow revelation of the metal distribution inside the cell and its internal structures. Understanding metal localization and distribution inside subcellular structures can be crucial in metal-based anticancer drug development. In recent years, the potential of LA-ICP-MS for the investigation of the uptake and distribution of metal-based anticancer compounds, either approved or under investigation, is being increasingly discussed in the literature and used for both monolayers of cells and tissue sections. To investigate the uptake and distribution of Pt, an area of 450 × 350 μm^2 containing between 15 and 40 TNBC MDA-MB-231 cells was analyzed using a laser beam with a circular diameter of 2 μm, a scan speed of 100 μm s^{-1}, and a laser repetition rate of 250 Hz.

Fig. 6 presents the $^{195}Pt^+$ signal intensity as a function of position and shows the distribution of Pt inside TNBC MDA-MB-231 cells after incubation with PtPCTZ, cisplatin or carboplatin. Signals above the LOD were detected within the cell areas only and, as clearly visible in the images, the spatial resolution obtained was sufficient to differentiate between the cell nucleus, cytosol, and background. LA-ICP-MS mapping thus confirms the cellular uptake of all Pt drug complexes tested. The $^{195}Pt^+$ signal intensities in the untreated control cells could not be distinguished from the gas background signal (Fig. S2†), as was also observed using LA-ICP-MS analysis of entire single cells.

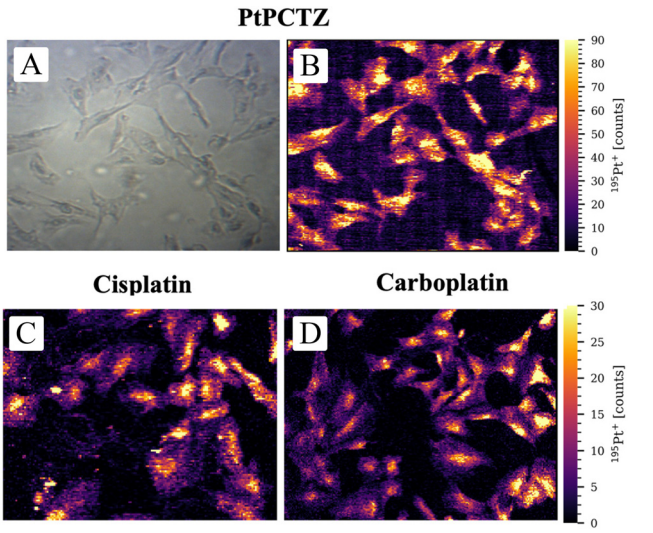

Fig. 6 (A) Selected region to perform image acquisition for the cells incubated with PtCTZ. (B–D) LA-ICP-MS maps displaying the $^{195}Pt^+$ signal intensity within single TNBC MDA-MB-231 cells after incubation for 24 h with 7 μmol L^{-1} PtPCTZ, 30 μmol L^{-1} cisplatin or 30 μmol L^{-1} carboplatin.

The maps or images obtained for the cells after exposure to the Pt-based drugs reveal that the nuclei are characterized by the highest $^{195}Pt^{+}$ signal intensities, indicating an elevated Pt concentration in this subcellular compartment. The nucleus is like the brain of the cell, because this is the location where the genetic instructions are initiated. It is where the chromosomes composed of molecules of deoxyribonucleic acid, DNA, are located, which carriy all the information about the characteristics of the species and participate in the hereditary mechanisms.[22] It is known that cisplatin, carboplatin and other Pt-based drugs form irreversible Pt-DNA adducts, which is thought to be the main reason for the cytotoxicity displayed by these drugs. The Pt metal center can coordinate to guanine bases from different DNA strands to form interstrand cross-links. The DNA lesion is then recognized by cellular machinery that either repairs the lesion, bypasses it, or initiates apoptosis. The most significant mechanism by which classical platinum complexes are believed to induce apoptotic cell death is inhibition of transcription.[23] The accumulation of PtPCTZ in the nuclei can be associated with DNA interaction, which should be the principal mechanism of action of this new complex, responsible for its cytotoxic activity towards the TNBC MDA-MB-231 cells.

Significantly higher accumulation of platinum was observed with cisplatin compared to the new drug PtCTZ. This difference is largely attributed to the different concentrations used during incubation; the concentration evaluated for PtCTZ was 7 μmol L^{-1}, which was significantly lower than the 30 μmol L^{-1} used for cisplatin. Despite lower concentrations inside the cells, PtCTZ exhibited good IC_{50} activity, indicating enhanced efficacy *in vitro*. These findings highlight PtCTZ as a promising candidate for further investigation in anticancer therapeutic research.

Experimental

Materials and methods

Cisplatin was purchased from Sigma-Aldrich (St Louis, MO, USA) and carboplatin from Strem Chemicals (Newburyport, MA, USA). Dulbecco's modified Eagle's medium (DMEM), RPMI medium 1640-GlutaMAXTM-I, fetal bovine serum (FBS), penicillin–streptomycin and trypsin-EDTA (0.05%) were purchased from Thermo Fisher Scientific (Rockford, IL, USA). Methylthiazolyldiphenyl-tetrazolium bromide (MTT), dimethylsulfoxide (DMSO), methanol, methylenechloride, K_2PtCl_4, triphenylphosphine, and NH_4PF_2 were purchased from Sigma-Aldrich. The MycoAlert Plus Kit was purchased from Lonza (Basel, Switzerland). Ultrapure water (18.2 MΩ cm) was obtained from a Milli-Q water purification system (Millipore, Bedford, MA, USA). Elemental analysis was performed using a FISIONS CHNS, mod. EA 1108 microanalyzer. The IR spectra were recorded using a FT-IR Bomem–Michelson 102 spectrometer in the range of 4000–250 cm^{-1} using KBr pellets. Conductivity data were obtained using a Meter Lab CDM2300 instrument. All the 1D and 2D NMR experiments (1H, 31P {1H}, 1H–1H gCOSY) were recorded with a 9.4 T Bruker Avance III 400 MHz spectrometer.

Synthesis

A dichloromethane solution of *cis*-$[PtCl_2(PPh_3)_2]$ (0.80 mmol, 50 mL) was stirred until dissolution in a Schlenk flask under an argon atmosphere. Subsequently, NH_4PF_6 (2.40 mmol) and CTZ (1.60 mmol) were added into the flask. The mixture was stirred and refluxed for 24 h, then the volume of solvent was reduced under vacuum and the solid obtained was washed with water and diethyl ether and dried under vacuum.

A white solid was obtained with a yield of 85%. Elemental analysis (%) calculated for $C_{58}H_{47}Cl_2N_2F_6P_3Pt$: C 55.96; H 3.81; N 2.25. Found: C 56.24; H 3.78; N 2.63. IR: ν(C–H aromatic) 3085 cm^{-1}, ν(C═N) 1572 cm^{-1}, ν(C═C) 1510 cm^{-1}, ν(P–F) 840 cm^{-1}, δ(P–F) 557 cm^{-1}, ν(Pt–P) 518 cm^{-1} and ν(Pt–Cl) 312 cm^{-1}. 1H NMR (acetone-d_6) δ ppm [(integral; multiplicity; assignation)]: 6.73 (1H, bs, H-imidazole), 6.83 (1H, bd, H-imidazole), 6.98 (4H, m, Cl-phenyl), 7.25; 7.37; 7.43; 7.49; 7.70 (40H, m, phenyl-CTZ and phenyl-PPh3), 8.06 (1H, bs, H-imidazole). $^{31}P\{^1H\}$ NMR (acetone-d_6) [δ ppm, (assignation, multiplicity, J Hz)]: −144.5 (PF_6, sept., $^1J_{P-F}$ = 710.11 Hz), 4.73 (PPh_3b, d, $^2J_{P-P}$ = 18.98 Hz, $^1J_{P-Pt}$ = 3315.24 Hz), 13.98 (PPh_3a, d, $^2J_{P-P}$ = 18.98 Hz, $^1J_{P-Pt}$ = 3653.03 Hz). Λ_M (acetone) = 107 ± 2 Ω^{-1} cm^2 mol^{-1}.

Cell culture

Cell culturing was performed at the Laboratory of Experimental Cancer Research of the Faculty of Medicine and Health Science at the Ghent University Hospital. The human mammary carcinoma cell line MDA-MB-231 GFP Luc (ATCC HTB-26) was maintained in DMEM supplemented with 10% FBS and antibiotics (100 IU mL^{-1} penicillin, 100 μg mL^{-1} streptomycin and 500 ng mL^{-1} doxycycline) and incubated at 37 °C under a 10% CO_2 humidified atmosphere and cultured under sterile conditions inside a class II biological safety cabinet. Cultures of this cell line were regularly tested for *Mycoplasma* using the MycoAlert Plus Kit. The results were negative for *Mycoplasma* contamination. Cells were separated by trypsinization at the time of use, counted and seeded according to the needs of each experiment. Cells were treated with different concentrations of the Pt-based complexes, according to each experiment performed. All results represent a minimum of three biological replicates.

Morphology and adherent conditions of tumour cells after exposure to metal complexes

The growth, confluence and morphology of the cells before and after treatment with the metal-based drugs were evaluated using a phase contrast microscope (Leica DMI3000B; Leica, Diegem, Belgium) and cell images were captured for each experiment (camera, Leica DF340FX).

MTT assay

MDA-MB-231 cells were seeded in 96-well plates (2×10^4 ^{C}ells per well) in 150 μL of media. After 24 h, the cells were treated

with the selected concentrations of the Pt-based complexes in sets of 9 replicates for each concentration. After drug exposure for 24 h, 40 μL of MTT (5 mg mL^{-1}) was added to each well and the plates were incubated for 2 h at 37 °C. The culture medium and the MTT reagent were removed, and 200 μL of DMSO was added to each well. Spectrophotometric readings were obtained at 570 nm using a Bio-Tek microplate reader instrument (Charlotte, NC, USA). Percent cell survival was determined as treated/untreated controls × 100.

Cell exposure experiments for LA-ICP-MS

Cells were seeded at 2 × 10^4 cells per well in 24-well clear bottom plates fitted with circular 13 mm diameter sterile coverslips. After 24 h, the culture medium was removed and fresh medium containing the selected concentration of the Pt-based complex was added. After 24 h of treatment, the medium was aspirated, and the cells were washed twice with 2 mL of Milli-Q water to ensure that each Pt-exposed well was cleaned appropriately. Afterwards, the cells were fixed using 0.2 mL of 3% PFA as the chemical fixative for 15 minutes, washed with Milli-Q water and dehydrated in an ascending ethanol series (25, 50, 70, 90 and 100%, 3 minutes each, 0.3 mL) and allowed to dry under a laminar flow. The coverslips were then transferred to a microscope slide using double-sided tape and stored at 2 °C until LA-ICP-MS analysis. The concentrations used were: 7.0 μmol L^{-1} of PtPCTZ and 30.0 μmol L^{-1} of cisplatin or carboplatin. A schematic representation of this exposure experiment is provided in Fig. 7.

LA-ICP-MS external calibration with homogeneous gelatin droplet standards

Platinum quantification in cells after exposure to anticancer Pt-based drugs was based on an external calibration approach with homogeneous gelatin droplet standards prepared following the protocol described by Šala *et al.*[24] The homogeneous 10% (m/v) gels containing 0, 0.1, 0.5, 1.0, 5.0, 10.0, 50.0 and 100.0 μg g^{-1} of Pt were prepared by spiking different amounts of a 1000 μg mL^{-1} Pt stock solution (Inorganic Ventures, Christiansburg, IL, USA) into microcentrifuge tubes containing 0.1 g of gelatin and diluting these mixtures with ultrapure water (Milli-Q, Millipore) to a total weight of 1.0 g. The suspensions were treated in a water bath at 60 °C for 1 h to obtain a clear solution. Drops of approximately 10 μL were deposited on a glass microscope slide and dried in a conventional oven at 95 °C for 1 h in a closed Petri dish. The resulting circular deposits are shown in Fig. S3.† Interferometric measurements were performed on the gelatin standards after spot ablation to determine the ablation crater volume as described by Van Acker *et al.*[15]

LA-ICP-MS instrumentation, settings and data acquisition conditions

The LA-ICP-MS setup included an Analyte G2 193 nm ArF* excimer-based LA system, equipped with a cobalt ablation chamber (Teledyne Photon Machines Inc., Omaha, NE, USA) and a low-dispersion tube-type ablation cell.[25] This ablation cell was coupled to the torch of an Agilent 7900 quadrupole-based ICP-mass spectrometer (Agilent Technologies, Tokyo, Japan) *via* the aerosol rapid introduction system (ARIS).[26–28] The ARIS was developed at Ghent University and is commercialized by Teledyne Photon Machines (Bozeman, MT, USA). Low-dispersion setups yield much shorter peak profiles (a single pulse response duration of <10 ms, FW0.1M), which is crucial for fast subcellular mapping applications.

The instrumental parameters were tuned and optimized for low oxide formation, low laser-induced fractionation and high sensitivity. Individual tumour cells were quantitatively ablated by firing a burst of 10 consecutive laser shots at a laser repetition rate of 250 Hz and a laser energy density of 0.22 J cm^{-2}, thereby generating one transient signal per ablated cell. A dwell time of 2 ms was selected. Only a single-mass channel was monitored (^{195}Pt) and the signal response was integrated per cell. The dried homogeneous gelatin in droplets was spot ablated in the same way as the cells using the same instrument settings and data acquisition conditions. In total, 10 spots were ablated per calibration standard and the average integrated $^{195}Pt^+$ signal intensities were used to construct the calibration curve as a function of the absolute masses of Pt. Optical interferometry was used to determine the ablated volume for each crater as described by Van Acker *et al.*[15] High spatial resolution LA-ICP-MS mapping was performed to visualize the Pt uptake and distribution in the membrane, cyto-

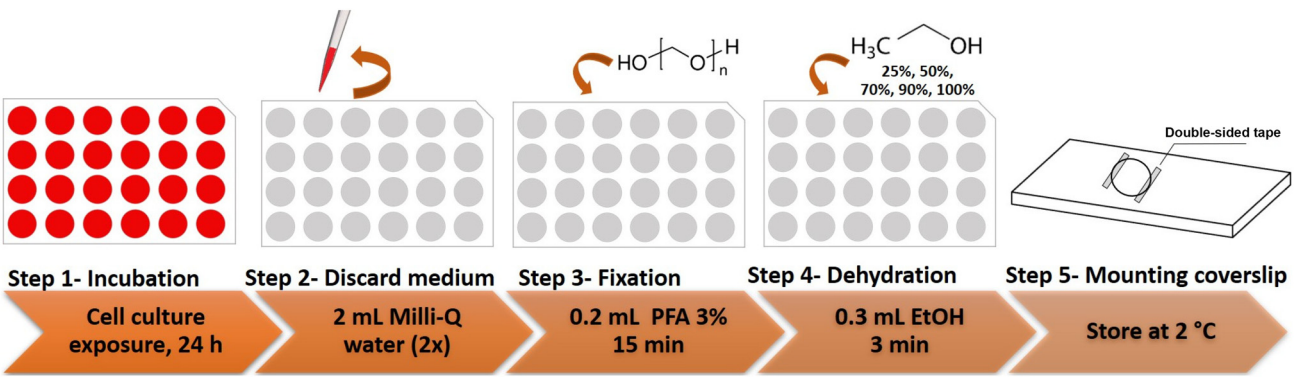

Fig. 7 Protocol for obtaining fixed and dehydrated TNBC MDA-MB-231 cells suited for analysis by LA-ICP-MS.

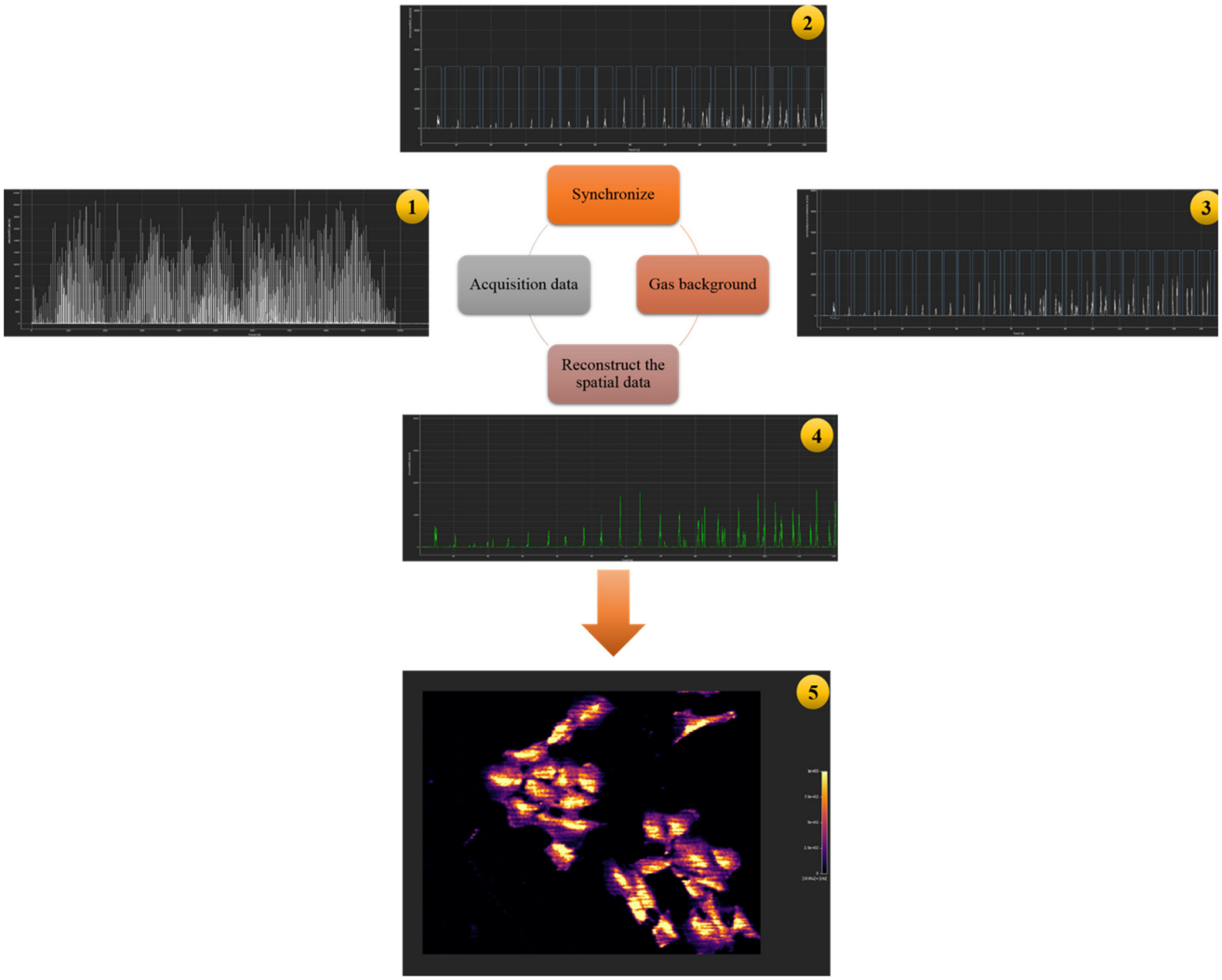

Fig. 8 Schematic representation of the subsequent steps in the HDIP software resulting in the reconstruction of cellular images.

plasm and/or the nucleus of adherent tumour cells. The instrument settings and data acquisition conditions used to analyze 450 × 350 μm^2 regions of interest were a laser beam with a circular diameter of 2 μm, a repetition rate of 250 Hz, an energy density of 0.33 J cm^{-2} and a lateral scan speed of 100 μm s^{-1}. A dwell time of 20 ms was selected for ^{195}Pt to achieve a pixel acquisition rate of 50 pixels s^{-1}.

Platinum quantification in single cells and processing of the Pt maps were performed using HDIP (HDF-based Image Processing) software designed to process imaging data stored in HDF5 format, a hierarchical data file format, and commercialized by Teledyne Photon Machines. The data reduction software was used to detect and integrate the peaks in the transient signal monitored using the region of interest (ROI) tool. Synchronization between the laser log files and the ICP-MS data files guarantees correct image analysis, which was performed using HDIP software. The data processing schematically shown in Fig. 8 includes a gas background subtraction and a reconstruction of the spatial data from the transient MS signal to a virtual grid.

Conclusions

The synthesized platinum(II) clotrimazole complex (PtPCTZ) exhibited notable cytotoxic activity, as evidenced by morphological changes and reduced cell viability. LA-ICP-MS analysis confirmed the cellular uptake of PtPCTZ, along with that of the reference drugs cisplatin and carboplatin. LA-ICP-MS was successfully used to determine platinum cellular uptake at the single cell level. Moreover, high spatial resolution LA-ICP-MS mapping revealed the distribution of the platinum-based anticancer drugs in TNBC MDA-MB-231 cells and demonstrated the accumulation of the compounds in the cell nucleus, indicating potential interaction of the new complex PtPCTZ with the DNA. Our findings obtained through LA-ICP-MS contribute to a better understanding of the cellular uptake and accumulation of new metal complexes inside tumour cells and shed some light on their most probable mechanism of action. Overall, our findings from this study illustrate the utility of LA-ICP-MS in bioinorganic and bioanalytical chemistry, par-

ticularly for the investigation of metal-based anticancer drugs. The ability to visualize and quantify metal distributions at the single-cell level offers valuable insights into the cellular mechanisms of action and can contribute to the development and optimization of new therapeutic metal drug agents.

Author contributions

L. C. V.: cell culture and sample preparation methodology, data curation and writing – original draft. T. V. A.: LA-ICP-MS data curation, formal analysis and writing, review & editing. W. V.: synthesis and characterization of PtPCTZ, and writing, review & editing. O. D. W.: cell culture resources and supervision, and writing, review & editing. A. A. B.: metal resources and validation, and writing, review & editing. J. A. N.: conceptualization, validation and writing, review & editing. F. V.: project administration, supervision and writing, review & editing.

Data availability

Data for this article, including LA-ICP-MS data, are available at the Open Science Framework at **https://osf.io/zmuhb/?view_only=6b1a7bea39f64f7c9054669fbc2d56ab**.

The data supporting this article have been included as part of the ESI.†

Conflicts of interest

F. V. is a co-inventor of patent WO2016042165A1, on which part of the technology of the cobalt ablation cell used in this work is based. T. V. A. and F. V. conduct research at a research unit that has licensed intellectual property to Teledyne Photon Machines.

Acknowledgements

The authors are grateful for the financial support provided by CNPq, CAPES and FAPESP (grant no. 2017/23254-9 and 2016/23130-5). F. V. and O. D. W. acknowledge the Flemish Research Foundation FWO for financial support in the form of research project G023521N. T. V. A. thanks the Research Foundation Flanders for support in the form of a postdoctoral research fellowship (FWO.3E0.2022.0048.01).

References

1 **https://www.cancer.gov/about-cancer/understanding/what-is-cancer**, NIH official site, accessed in June 2024.
2 **https://www.who.int/news-room/fact-sheets/detail/cancer**, OMS official site, accessed in June 2024.
3 H. Borghaei, M. R. Smith and K. S. Campbell, *Eur. J. Pharmacol.*, 2009, **625**, 541.
4 J. Guo, B. Xu, Q. Han, H. Zhou, Y. Xia, C. Gong, X. Dai, Z. Li and G. Wu, *Cancer Res. Treat.*, 2018, **50**, 445.
5 C. A. Puckett, R. J. Ernst and J. K. Barton, *Dalton Trans.*, 2010, **39**, 1159.
6 J. S. Becker, *Inorganic mass spectrometry*, Wiley, Chichester, 2007.
7 S. J. M. Van Malderen, E. Vergucht, M. D. De Rijcke, C. Janssen, L. Vincze and F. Vanhaecke, *Anal. Chem.*, 2016, **88**, 5783.
8 D. Drescher, C. Giesen, H. Traub, U. Panne, J. Kneipp and N. Jakubowski, *Anal. Chem.*, 2012, **84**, 9684.
9 S. Böhme, J. H. Stärk, T. Meißner, A. Springer, T. Reemtsma, D. Kühnel and W. Busch, *J. Nanopart. Res.*, 2014, **16**, 2592.
10 T. Buckle, S. van der Wal1, S. J. M. van Malderen, L. Müller, J. Kuil, V. van Unen, R. J. B. Peters, M. E. M. van Bemme, L. A. McDonnell, A. H. Velders, A. F. Koning, F. Vanhaecke and F. W. B. van Leeuwe, *Theranostics*, 2017, **7**, 624.
11 T. Van Acker, T. Buckle, S. J. M. Van Malderen, D. M. van Willigen, V. van Unen, F. W. B. van Leeuwen and F. Vanhaecke, *Anal. Chim. Acta*, 2019, **1074**, 43.
12 A. J. Managh and C. Greenhalgh, Imaging of Subcellular Distribution of Platinum in Single Cells Using Laser Ablation Inductively Coupled Plasma Mass Spectrometry. in *Single Cell Analysis Methods and Protocols*, ed. M. Gužvić, Humana, 2024, pp. 215–226, ISBN: 9781071636206.
13 M. Z. Koh, W. Y. Ho, S. K. Yeap, N. M. Ali, L. Boo and N. B. Alitheen, *Pharmaceuticals*, 2021, **14**(5), 391.
14 B. W. Darvell, in *Materials Science for Dentistry*, 10th edn, 2018, ch. 3, Polymers.
15 T. Van Acker, S. J. M. Van Malderen, L. Colina-Vegas, R. K. Ramachandran and F. Vanhaecke, *J. Anal. At. Spectrom.*, 2019, **34**, 1957.
16 J. Zhu and C. B. Thompson, *Nat. Rev. Mol. Cell Biol.*, 2019, **20**, 436.
17 W. Stallaert, S. R. Taylor, K. M. Kedziora, C. D. Taylor, H. K. Sobon, C. L. Young, J. C. Limas, J. V. Holloway, M. S. Johnson, J. G. Cook and J. E. Purvis, *Mol. Syst. Biol.*, 2022, **18**, e11087.
18 A. E. Egger, C. Rappel, M. A. Jakupec, C. G. Hartinger, P. Heffeter and B. K. Keppler, *J. Anal. At. Spectrom.*, 2009, **24**, 51.
19 M. C. Rodríguez, R. A. F. García, E. B. Gonzalez, J. Bettmer and M. Montes-Bayon, *Anal. Chem.*, 2017, **89**, 11491.
20 S. Pillozzi and A. Arcangeli, *Br. J. Cancer*, 2018, **118**, 200.
21 Z. Wang, H. Yu, S. Gou, F. Chen and L. Fang, *Inorg. Chem.*, 2016, **55**, 4519.
22 T. Guo and Y. Fang, *Front. Plant Sci.*, 2014, **5**, 378.
23 S. Ghost, *Bioorg. Chem.*, 2019, **88**, 102925.
24 M. Šala, V. S. Šelih and J.T. van Elteren, *Analyst*, 2017, **142**, 3356.

25 S. J. M. Van Malderen, J. T. van Elteren and F. Vanhaecke, *J. Anal. At. Spectrom.*, 2015, **30**, 119.
26 T. Van Acker, S. J. M. Van Malderen, T. Van Helden, C. Stremtan, M. Šala, J. T. van Elteren and F. Vanhaecke, *J. Anal. At. Spectrom.*, 2021, **36**, 1201.
27 S. J. M. Van Malderen, A. J. Managh, B. L. Sharp and F. Vanhaecke, *J. Anal. At. Spectrom.*, 2016, **31**, 423.
28 S. J. M. Van Malderen, E. Vergucht, M. De Rijcke, C. Janssen, L. Vincze and F. Vanhaecke, *Anal. Chem.*, 2016, **88**, 5783.